https://doi.org/10.1038/s44386-026-00038-5

Preferential HER4 stimulation preserves neuregulin-induced improvement of myocardial function

Samuel L. Murphy[1] ✉, Wai Hong Wilson Tang[2], Xiaolei Zhuang[1] & John Li[1]

Neuregulin-1 (NRG-1), the natural ligand for HER3 and HER4, has been established as an essential growth factor for heart function. Prior studies have demonstrated the therapeutic potential of NRG-1 in the treatment of heart failure, but HER3 receptor activation has been a concern given its cancer association. Here, we describe the novel antibody fusion protein JK07, consisting of an antagonistic HER3 antibody and the EGF-binding domain of NRG-1. We confirm the HER3 antibody and the NRG-1 domains both retain functional activity in vitro and in vivo. Importantly, we demonstrate here for the first time that preserving HER4 stimulation by NRG1 in the presence of attenuated HER3 stimulation is sufficient to realize the therapeutic effects of NRG-1 in treatment of heart failure. Comparing JK07 to a control NRG-1 antibody fusion which does not recognize HER3, we show that JK07 can achieve equivalent recovery of ejection fraction in a rodent model of chronic heart failure. Finally, JK07 exhibited therapeutic potential in heart failure in rhesus macaques. In conclusion, this work demonstrates selective HER4 activation is sufficient for NRG-1 to improve myocardial function in multiple pre-clinical heart failure models and that JK07 holds promise as a potential therapeutic intervention for heart failure.

Despite the establishment of available guideline-directed medical therapies[1], heart failure remains one of the leading causes of morbidity and mortality globally[2]. Approximately half of heart failure patients survive beyond five years following their initial diagnosis[3], compelling continued research and development of new therapies, and in particular, identification of new mechanisms of action that might more directly impact the disease pathophysiology and serve to complement currently available treatments.

Neuregulins are members of the epidermal growth factor (EGF) family. Neuregulin-1 (NRG-1), in particular, is important for the development, homeostasis, and repair of the myocardium[4]. The isoforms of NRG-1 all share a common EGF-like domain essential for its biological activity[5]. NRG-1 binds directly to the human EGF receptors human epidermal growth factor 3 (HER3) and/or HER4 (also known as ErbB3 and ErbB4)[6]. Binding of neuregulin to either HER3 or HER4 induces receptor dimerization, with HER2, which in most cases is required for subsequent induction of intracellular signaling initiated by phosphorylation of the cytoplasmic tail[7,8]. Pathways activated by the HER2/HER4 signaling complex include PI3K/AKT, MEK/ERK, VEGF, Hippo/YAP, and FAK[9].

An appreciation for the clinical significance of neuregulins in heart function arose from the observations that the use of trastuzumab, which blocks HER2 signaling, can cause left ventricular dysfunction[10], and that use of trastuzumab in combination with cardiotoxic anthracyclines increased the frequency of left ventricular dysfunction[11,12]. This myocardial dysfunction was directly linked to reduced HER4 signaling mediated by NRG-1[13]. Based on these observations, which suggest that neuregulin has a clinically relevant role in myocardial maintenance and repair, the use of recombinant neuregulin (rNRG) was explored extensively in pre-clinical models of heart failure, including those induced by post-myocardial infarction, chronic rapid pacing, viral myocarditis, and doxorubicin[11,13–16]. With the consistent demonstration of therapeutic effects across a panoply of animal models, rNRGs have also been evaluated clinically for the treatment of heart failure. In a Phase 1b study, a full-length rNRG, called cimaglermin, was evaluated in the treatment of patients with heart failure with reduced ejection fraction (HFrEF) and New York Heart Association (NYHA) II to III symptoms[17]. Following a single administration, the high-dose groups of the study exhibited an average improvement in left ventricular ejection fraction (LVEF) of >8% absolute (>30% relative improvement) 90 days after a single dose of cimaglermin. This finding was reinforced by studies showing that another investigational therapeutic, Neucardin[18], a smaller rNRG peptide fragment encompassing the EGF binding domain, showed similar, although more modest, improvement in myocardial function.

[1]Salubris Biotherapeutics, Inc., Gaithersburg, MD, US. [2]Cleveland Clinic, Cleveland, OH, US. ✉e-mail: sam.murphy@salubrisbio.com

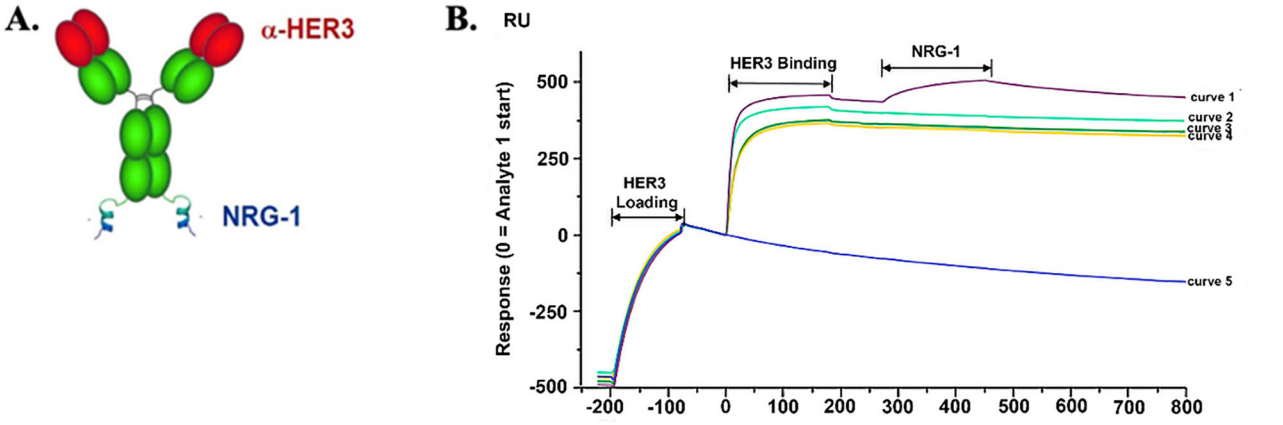

Curve	Injected Sample	
	HER3 Binding	NRG-1 Binding
1	JK07	NRG-1 mAb
2	JK07	Buffer
3	HER3 antagonist antibody	NRG-1 mAb
4	HER3 antagonist antibody	Buffer
5	Buffer	Buffer

Fig. 1 | Structure of JK07. A Schematic of JK07 structure. **B** SPR sensorgram.

Exploitation of the therapeutic effects of rNRG has been constrained by dose-limiting gastrointestinal (GI) toxicities[18], and, in the case of cimaglermin, hepatotoxicity, which was observed in the Phase 1-enabling animal toxicity work and was dose-limiting in the Phase 1b study[17]. Moreover, concerns arose over the risk that rNRG treatments for heart failure could exacerbate pre-existing but undetected cancers. The risk of cancer was primarily related to rNRG activation of HER3, which is a well-established driver of cancer progression[19], and not to rNRG activation of HER4, which has not definitively been associated with cancer[20]. Recent evidence has emerged that oncogenic *NRG-1* fusions occur in several cancers[21,22], and targeted therapeutics specific for HER3 have shown considerable promise in the treatment of such NRG fusion cancers[23]. Based on this and the additional hypothesis that HER3 signaling prevalent in the GI tract could be the primary driver of GI toxicity, the potential benefits of a HER4-selective agonist have been proposed previously[24]. However, to date, it has not been shown whether attenuation of HER3 signaling would impact the ability of NRG-1 to improve and sustain myocardial function.

We set out to address this uncertainty through the creation of JK07, an antibody fusion protein consisting of an antagonistic HER3-specific antibody and C-terminal fusion domains encompassing the EGF-binding domain of NRG-1 in a homodimeric configuration. JK07 was designed to selectively and preferentially stimulate HER4 over HER3 signaling, which we verify here through both in vitro and in vivo studies, including a xenograft model. We subsequently show that selectivity for HER4 does not diminish the potential of JK07 to improve myocardial function in comparison to a control antibody fusion protein in a rat ligation model of heart failure. Finally, we demonstrate that JK07 can improve myocardial function in a spontaneous model of heart failure in rhesus macaques, including animals with both reduced and preserved ejection fraction.

Results

A recombinant fusion protein consisting of a fully human monoclonal antibody that antagonizes HER3 and an active recombinant polypeptide fragment of the human NRG-1 was designed (JK07). The EGF-like domain of NRG-1 was fused to the C-terminus of the antibody heavy chain via a G4S linker in a homodimeric configuration (Fig. 1A). JK07 is specifically designed to block NRG-1-mediated HER3 signaling activation while preserving NRG-1-mediated HER4 activation and function. The antibody end is derived from patritumab, which has been tested in clinical development in the treatment of HER3-associated cancers, and used as the scaffold for multiple bispecific drug candidates in development. The EGF-like domain is a 60aa sequence based on human NRG-1 protein (Uniprot # Q02297). JK07 showed purity of >99% by size exclusion chromatography.

JK07 Efficiently Binds HER3 While Preserving Structural Integrity of NRG-1 Fusion

We first sought to confirm the binding specificity of the JK07 molecule through a surface plasmon resonance (SPR) technology-based assay. A His-tagged HER3 recombinant protein was captured on the sensor chip by an anti-His antibody, and binding was visualized as an increase in signal (Fig. 1B, HER3 Loading). The sequential injection of JK07 and an NRG-1-specific antibody yielded two additional increases in signal (Fig. 1B, HER3 Binding and NRG-1 Binding, respectively, curve 1), confirming the presence of both the HER3-binding domain and a structurally intact NRG-1 fragment within the JK07 molecule. In contrast, the addition of the HER3 antagonist antibody without the NRG-1 fusion domains followed by an NRG-1 antibody resulted in the lack of an NRG-1 binding peak (Fig. 1B, curve 3).

JK07 Attenuates HER3-dependent Activities in vitro and Demonstrates Anti-tumor Efficacy in vivo

To demonstrate that JK07 can directly suppress HER3-dependent activities, we employed a U2OS ErbB2/ErbB3 Dimerization Cell Line (Eurofins DiscoverX) to assess ligand-induced dimerization (Fig. 2A). Compared to recombinant ligand NRG-1 alone, JK07 showed a significantly reduced signal, supporting that the anti-HER3 antibody

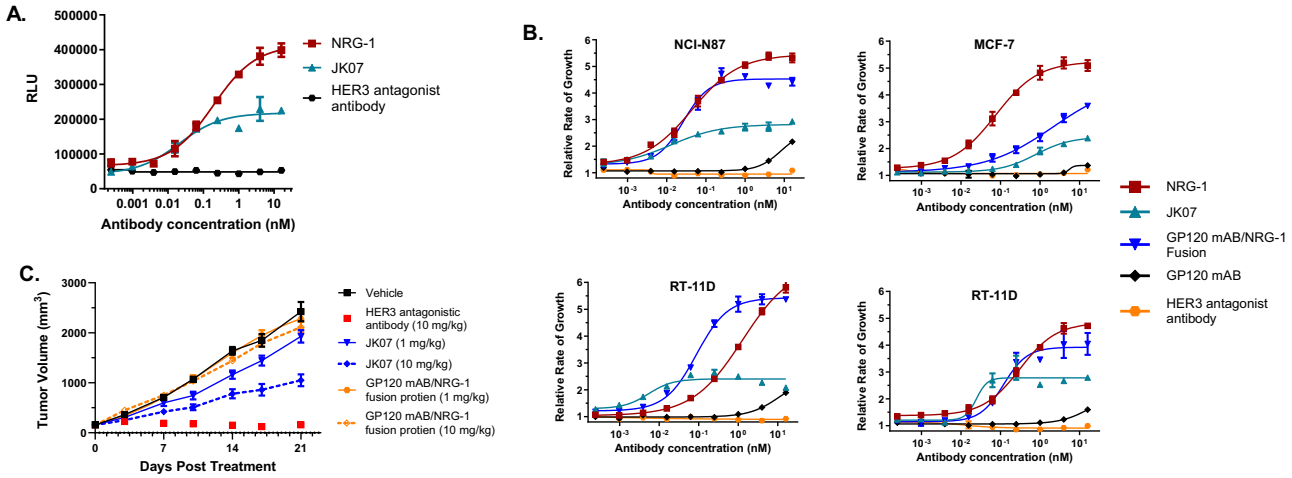

Fig. 2 | JK07 HER3 Antagonism Functional Assessment. A HER2/HER4 dimerization in U2OS HER2/HER4 dimerization cell lines. **B** In vitro proliferation assay evaluating JK07 activity in promoting cancer cell growth (NCI-N87, MCF07, RT-11D and T47D) driven by the HER3 signaling pathway. Results are representative of three independent experiments. **C** Evaluation of JK07 in a subcutaneous FaDu carcinoma xenograft model in NOD/SCID mice. Results were statistically significant at Day 21 for HER3 antagonistic antibody ($p < 0.001$), JK07 1 mg/kg ($p < 0.05$), and JK07 10 mg/kg ($p < 0.001$).

component of JK07 is capable of inhibiting NRG-1-induced receptor dimerization and activation.

Previous in vitro research has shown that the HER2/HER3 signaling pathway is a driver of the proliferation of several cancer cell lines under serum-free conditions, including NCI-N87 human gastric cancer cells, RT-112 human bladder tumor cells, and MCF-7 and T47D human breast cancer cells. We hypothesized that the anti-HER3 antibody would impair proliferation of these cell lines. Therefore, an in vitro proliferation assay was performed to examine the activity of JK07 in promoting or suppressing cancer cell growth. an anti-HER3 antibody, an irrelevant antibody (GP120 mAB recognizing HIV Envelope protein gp120), and an anti-gp120/NRG1 fusion protein (GP120 mAB/NRG-1 fusion). Across four cancer cell lines (Fig. 2B), JK07 consistently showed lower level of proliferation induction in comparison to NRG-1 and the gp120/NRG-1 fusion, while the level of reduction by JK07 varies among different cancer cell lines. The HER3 antibody and the gp120 antibody induced the lowest levels of proliferation, less than JK07 (Fig. 2B), suggesting there is some preserved, though attenuated, HER2/HER3 activation with JK07.

Based on these in vitro results, we sought to further evaluate the potential of JK07 to inhibit HER3-mediated cancer cell proliferation in vivo. To do this, we selected the FaDu xenograft model, as FaDu cells are primarily driven by the HER3 signaling pathway[25]. Mice were first inoculated with FaDu cells, and ten days after the tumor inoculation, the mean tumor volume reached 154 mm3, at which time tumor-bearing mice were randomized and received the first dose of treatment (Day 0). The mean tumor volume in the vehicle control group reached 2422.3 mm3 on Day 21. The HER3 antibody exhibited nearly complete tumor growth inhibition (TGI), showing a mean tumor volume of 157.8 mm3 or a TGI of 93.5% ($p < 0.001$ vs. vehicle control group) on Day 21 post-treatment (Fig. 2C), confirming that the growth of FaDu carcinoma xenograft tumor is driven by the HER3 signaling pathway. Treatment of tumor-bearing mice with JK07 resulted in a statistically significant and dose-dependent tumor growth inhibition at Day 21 post-treatment: 19.2% at 1 mg/kg dosage ($p = 0.048$ vs. vehicle group) and 56.2% at 10 mg/kg dosage ($p < 0.001$ vs. vehicle group) (Fig. 2C). The anti-gp120/NRG-1 fusion protein showed no suppression of tumor growth relative to vehicle at either matched dose level (Fig. 2C). These data demonstrate that the HER3-specific antibody domain of JK07 can inhibit HER3 receptor activation and significantly attenuate tumor growth in an in vivo cancer model. No differences in weight gain or loss were observed between any of the treatment groups (data not shown).

JK07 Preserves NRG-1-Mediated HER2/HER4 Dimerization and Signal Activation

Following the demonstration that the JK07 suppressed HER3 signaling in vitro and in vivo, we next sought to confirm the retention of HER2/HER4 signaling induction by the NRG-1 fusion domain. To measure specific HER4 dimerization, a receptor dimerization assay was performed using an U2OS ErbB2/ErbB4 Dimerization Cell Line. JK07 induced HER2/HER4 dimerization with potency comparable to recombinant NRG-1 (Fig. 3A).

To confirm activation of signaling pathways induced by HER2/HER4 dimerization in cardiomyocytes following exposure to JK07, AKT phosphorylation was evaluated by ELISA analysis in induced human pluripotent stem cell-derived cardiomyocytes which express HER2 and HER4, but not HER3. AKT phosphorylation increased in a dose-dependent manner with JK07, with a potency similar to recombinant NRG-1 (Fig. 3B). AKT phosphorylation also increased when cells were exposed to anti-gp120/NRG-1, but not with anti-HER3 or anti-gp120 antibodies without the NRG-1 fusion (Fig. 3B). Western blot analysis mirrored these results. Exposure of human and rat cardiomyocytes to rNRG-1, JK07 or gp120 mAb/NRG1 fusion, increased the phosphorylation of AKT, whereas HER3 or gp120 mAb alone did not induce AKT phosphorylation in both cell types (Fig. 3C, D).

JK07 Restores Cardiac Function in a Rodent Model of Chronic Heart Failure with reduced Ejection Fraction (HFrEF)

To evaluate JK07 therapeutic effects in comparison to NRG-1, we first used a ligation model for chronic HFrEF. Sprague-Dawley rats were anesthetized with an intraperitoneal injection of 60 mg/kg of 3% pentobarbital sodium and underwent left anterior descending (LAD) coronary ligation procedures. Four weeks after LAD ligation, animals with reduced EF (>30% decrease from baseline) were randomized and assigned into five groups with 11 animals per group as follows: a vehicle control group, a positive control group, and JK07 cohorts of 1, 3 and 10 mg/kg, respectively. Ten animals undergoing sham surgery (i.e., no ligation) were included in the sham control group. Animals in the vehicle control group and the sham control group were administered PBS during the treatment period; animals in the positive control group were administered 10 mg/kg gp120/NRG-1.

All animals received administration twice per week for up to four weeks. As decreased body weight and increased mortality were observed at higher JK07 dose levels, the number of doses administered was reduced at the mid- and high-dose levels of the study. Animals received a total of eight doses of JK07 at the 1 mg/kg dose level, six doses at the 3 mg/kg dose level, and three doses at the 10 mg/kg dose level, respectively. Separate studies

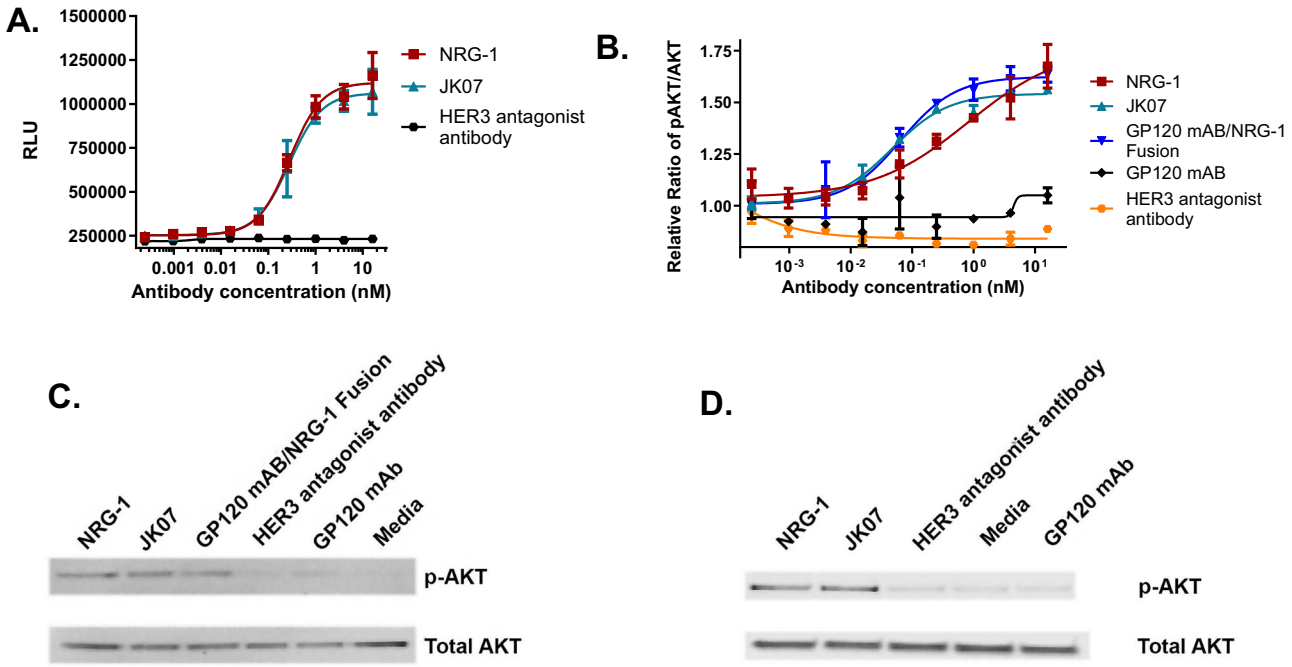

Fig. 3 | JK07 HER4 Agonism Functional Assessment. A HER2/HER4 dimerization in U2OS HER2/HER4 dimerization cell lines. **B** AKT phosphorylation by ELISA **C** and by Western blot in human IPS-induced cardiomyocytes. **D** AKT phosphorylation by Western blot in rat cardiomyocytes. All results are representative of three or more independent experiments.

Table 1 | Ejection fraction changes following treatment in a rodent model of chronic heart failure

Group	Baseline	Pre-treatment	Post-treatment		ΔEF (%)	
			W2	W4	W2	W4
Sham Control	95 ± 1.9	93.4 ± 4.0	92.9 ± 4.3	91.3 ± 5.3	-0.5 ± 2.6	-2.2 ± 3.2
Vehicle Control	93.5 ± 3.3	55.8 ± 8.3$^{\triangle\triangle\triangle}$	54.6 ± 10.1$^{\triangle\triangle\triangle}$	49.3 ± 10.2$^{\triangle\triangle\triangle}$	-1.8 ± 14.0	-10.5 ± 18.5
JK07 (1 mg/kg)	93.5 ± 3.5	56.8 ± 6.0$^{\triangle\triangle\triangle}$	65.7 ± 6.4	64.6 ± 7.5	16.2 ± 15.9**	14.7 ± 21.3***
JK07 (3 mg/kg)	93.8 ± 2.7	55.0 ± 7.3$^{\triangle\triangle\triangle}$	68.4 ± 8.3	67.5 ± 11.7	26.3 ± 13.7***	26.9 ± 13.2***
JK07 (10 mg/kg)	94.0 ± 3.1	54.7 ± 7.5$^{\triangle\triangle\triangle}$	71.7 ± 5.9	73.9 ± 12.1	33.2 ± 20.0***	36.6 ± 23.0***
Positive Control	93.6 ± 3.2	55.2 ± 6.1$^{\triangle\triangle\triangle}$	66.1 ± 6.8	72.0 ± 9.5	19.8 ± 9.1**	28.8 ± 15.5***

Note: 1. W2: 2 weeks after the first administration; W4: 4 weeks after the first administration.
2. $^{\triangle\triangle\triangle}$denotes the significance level $p < 0.001$, compared to the sham control.
3. ***denotes the significance level $p < 0.001$, compared to the vehicle control.
4. **denotes the significance level $p < 0.05$, compared to the vehicle control.
5. $\Delta EF\ (\%) = [(EF_{post\text{-}treatment} - EF_{pre\text{-}treatment}) / EF_{pre\text{-}treatment}] \times 100\%$.

have demonstrated that mortality in rats relates to prolonged hypoglycemia induced by sustained exposure to the NRG-1 fusion domain (data not shown). Hypoglycemia is a known effect of NRG-1 in lower-order mammalian species[26].

Following the LAD coronary artery ligation, LVEF in test animals was reduced by 35-40% absolute from the corresponding baseline, demonstrating the successful establishment of the HFrEF model (Table 1). In the treatment phase (post-treatment), LVEF in the vehicle control group continued to deteriorate over time, whereas JK07 induced a significant and dose-dependent improvement in LVEF (Table 1), with peak increase in LVEF at 4 weeks of 15%, 27% and 37% at the 1, 3, and 10 mg/kg dose levels respectively. Similarly, anti-gp120/NRG-1 at 10 mg/kg increased the LVEF by 29% at 4 weeks post-treatment.

After the LAD coronary artery ligation, the left ventricular internal dimension at end-diastole (LVIDd) in test animals was enlarged by approximately 30% over baseline (Table 2). In the vehicle control group, the LVIDd continued to enlarge in the treatment phase, whereas in the groups receiving JK07 treatment at low, medium and high doses, LVIDd was reduced by 3.4, 9.8, and 10.1% after 2 weeks following the first dosing, and 0.6, 0.6 and 3.5% after 4 weeks. These improvements were statistically significant as compared to the vehicle control. Similarly, the LVID at end-systole (LVIDs) in LAD-ligated animals was increased by 2-3 fold over the baseline. In the vehicle control group, the LVIDs continued to deteriorate in the treatment phase. In contrast, treatment with JK07 resulted in a statistically significant, dose-dependent and sustained improvement on LVIDs (Table 2). As with the LVEF increase, these changes were comparable between JK07 at 10 mg/kg and the anti-gp120/NRG-1 fusion at 10 mg/kg.

To assess the impact of treatment on functional capacity, exercise endurance was evaluated using an exercise wheel and ten minute period of assessment. As shown in Table 3, JK07 treatment resulted in a statistically significant improvement in exercise capacity at the low dose. Although numerically superior to the control group, the mid and high dose levels as well as the positive control group failed to show a statistically significant improvement in exercise capacity.

To further evaluate potential structural changes in connection with the functional changes observed, histopathology analysis of the myocardium

Table 2 | Cardiac remodeling following treatment in a rodent model of chronic heart failure

Group	Baseline LVIDd	Pre-treatment LVIDd	Baseline LVIDs	Pre-treatment LVIDs	ΔLVIDd		ΔLVIDs	
					W2	W4	W2	W4
Sham Control	5.94 ± 0.36	7.04 ± 1.00	1.70 ± 0.38	2.21 ± 0.82	-0.24 ± 0.80	-0.09 ± 0.88	0.00 ± 0.50	0.19 ± 0.37
Vehicle Control	6.40 ± 0.69	8.43 ± 0.89$^{\triangle\triangle}$	2.01 ± 0.61	5.88 ± 0.97$^{\triangle\triangle\triangle}$	0.85 ± 0.88*	0.87 ± 1.04*	0.62 ± 0.60	0.96 ± 1.13
JK07 (1 mg/kg)	6.54 ± 0.46	8.26 ± 0.77$^{\triangle\triangle}$	2.04 ± 0.42	5.68 ± 0.63$^{\triangle\triangle\triangle}$	-0.28 ± 0.97**	-0.06 ± 0.55*	0.67 ± 0.97***	0.48 ± 0.92***
JK07 (3 mg/kg)	6.47 ± 1.01	8.34 ± 0.85$^{\triangle\triangle}$	1.99 ± 0.56	5.87 ± 0.91$^{\triangle\triangle\triangle}$	-0.82 ± 1.22***	-0.20 ± 1.09*	1.29 ± 0.98***	1.06 ± 1.06***
JK07 (10 mg/kg)	6.14 ± 0.58	8.59 ± 0.60$^{\triangle\triangle\triangle}$	1.86 ± 0.54	6.04 ± 0.65$^{\triangle\triangle\triangle}$	-1.1 ± 1.05***	-0.54 ± 0.93**	1.72 ± 0.87***	1.65 ± 1.27***
Positive Control	6.34 ± 0.46	8.49 ± 0.53$^{\triangle\triangle\triangle}$	1.97 ± 0.48	5.94 ± 0.53$^{\triangle\triangle\triangle}$	0.14 ± 0.99	-0.57 ± 1.26**	0.58 ± 0.66***	1.39 ± 0.90***

Note: 1. W2: 2 weeks after the first administration; W4: 4 weeks after the first administration.
2. $^{\triangle\triangle}p < 0.01$ and $^{\triangle\triangle\triangle}p < 0.001$ denote statistical significance in comparison to the sham control.
3. $^{*}p < 0.05$, $^{**}p < 0.01$, and $^{***}p < 0.001$ denote statistical significance in comparison to the vehicle control.
4. $\Delta LVIDd = LVIDd_{post\text{-}treatment} - LVIDd_{pre\text{-}treatment}$.
5. $\Delta LVIDs = LVIDs_{post\text{-}treatment} - LVIDs_{pre\text{-}treatment}$.

Table 3 | Effect of JK07 on exercise endurance (Mean ± SD)

Group	Dose (mg/kg)	Distance (m)
Sham Control	-	82.8 ± 21.2
Vehicle Control	-	44.0 ± 17.1$^{\triangle\triangle}$
JK07	1	76.9 ± 25.5*
JK07	3	52.1 ± 33.5
JK07	10	65.2 ± 38.9
Positive Control	10	58.4 ± 39.2

Note: 1. Exercise endurance was examined at 4 weeks after the first administration.
2. $^{\triangle\triangle}p < 0.01$ denotes statistical significance in comparison to the sham control.
3. $^{*}p < 0.05$ denotes statistical significance in comparison to the vehicle control.

was performed at 4 weeks after the first administration. In the sham control group, the cardiomyocytes had a well-organized spatial arrangement, and the cytoplasm and the myocardial fibers were evenly stained. No inflammatory cell infiltration was observed in the interstitial spaces, and no myocardial necrosis was observed (Fig. 4A). In contrast, in the vehicle control group, the myocardial infarction marginal zone exhibited widened gaps between myocardial cells; the nuclei were condensed and shattered, and the myocardial fiber arrangement lost its ordered structure; cardiomyocyte hypertrophy and interstitial edema were evident (Fig. 4B). Treatment with JK07 partially alleviated the pathological changes in the myocardial infarction zone in a dose-dependent manner, including a significant reduction of necrotic cells, narrowed interstitial spaces between myocardial cells, and recovery of myocardial fiber arrangement towards normal structure (Fig. 4D–F). No difference in recovery of tissue architecture was apparent in comparing JK07 treated animals with gp120/NRG-1 treated animals at a matched dose level of 10 mg/kg (Fig. 4C, F).

To detect potential changes in collagen content, an indicator of fibrosis, immunohistochemical staining was used to detect collagen type I and collagen type III within the myocardial infarction marginal zone. Expression levels of myocardial collagen type I and type III in the myocardial infarction marginal zone were markedly and significantly increased in the vehicle control as compared to the sham control (Table 4). Type I/III ratio was also increased significantly in the vehicle control group. At 4 weeks after the first administration JK07 of 1, 3, and 10 mg/kg, expression of collagen type I was downregulated by 6.6%, 37.1%, and 40.5%, respectively, as compared to the vehicle control; and the collagen I/III ratio also decreased by 4.7%, 40.8%, and 36.6%, respectively, relative to the vehicle control (Table 4). In contrast, JK07 showed no significant effect on the expression of collagen type III. Again in this analysis, gp120-NRG1 fusion performed similarly to JK07 at a matched dose of 10 mg/kg.

JK07 Improves Cardiac Function in Naturally Occurring Heart Failure in Rhesus Macaques with Either Reduced or Preserved Ejection Fraction

To further evaluate the potential for JK07 to improve myocardial function in heart failure with either reduced or preserved ejection fraction, a spontaneous model of heart failure in rhesus macaques was employed. Full details on this disease model can be found in materials and methods. Briefly, 26 rhesus monkeys with spontaneous chronic heart failure were shown to have disease characteristics that are very similar to heart failure patients, including cardiac remodeling (left atrial enlargement, left ventricular dilatation, etc.), cardiac dysfunction, diffuse myocardial fibrosis, continuously increased plasma N-terminal pro b-type natriuretic peptide (NT-proBNP), decreased daily activity and shortness of breath, etc. In addition, the criteria used for the classification of diastolic dysfunction in monkeys with chronic heart failure are in accordance with clinical standards. Overall, the rhesus monkey model of spontaneous chronic heart failure provides a highly analogous animal model system for the human condition of heart failure. In these studies, animals were treated with placebo, JK07, or the control molecule sacubitril/valsartan at the human equivalent dose level.

Thirteen of 26 (50%) animals were confirmed to have HFrEF disease. In the animals with HFrEF receiving vehicle control, no changes were observed in LVEF between baseline at the end of the dosing period and the end of the study. One animal included in the vehicle control group died on Day 18 of the study due to acute heart failure. Of the remaining five animals, none showed more than a 2% absolute change in LVEF during the study. Treatment with sacubitril/valsartan and JK07 both resulted in statistically significant improvement in a majority of the animals in the studies (Fig. 5), with seven of ten responding following JK07 treatment, and eight of ten responding following sacubitril/valsartan (6.6 mg/kg/day, human equivalent dose) treatment. JK07 treatment yielded a maximal response of at least 5% absolute increase in LVEF in seven of ten animals, at least a 10% absolute increase in ejection fraction in three of ten animals, and a maximum absolute improvement of 19.6% during the study. Similarly, following sacubitril/valsartan treatment, a maximal response of at least 5% absolute increase in LVEF was seen in seven of ten animals, at least a 10% absolute increase in LVEF in three of ten animals, and a maximum absolute improvement of 19.1% during the study. No significant changes in NTproBNP were observed across treatment groups.

In the 13 animals determined to have heart failure with preserved ejection fraction (HFpEF), changes were evaluated according to the diastolic

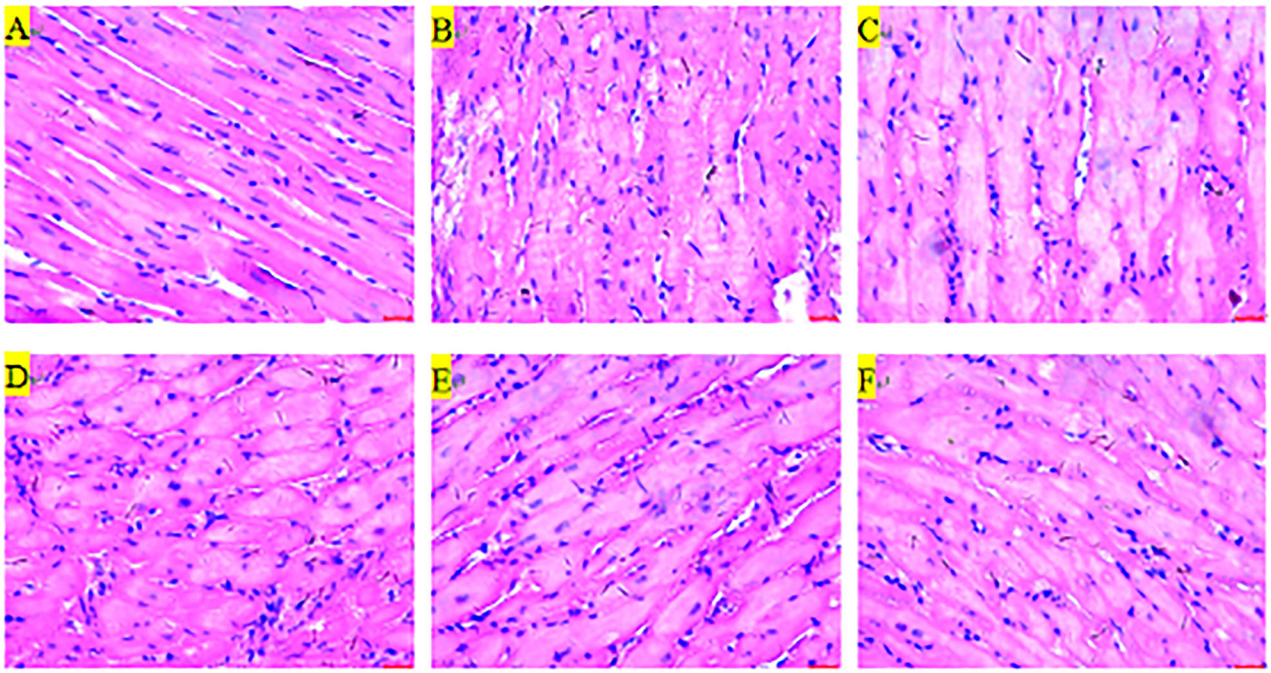

Fig. 4 | Histological Assessment of JK07-Mediated Myocardial Remodeling. A–F Fig. 4. Histopathological changes in cardiac muscle structure induced by JK07 in rats with systolic heart failure. Cardiac tissues were collected and fixed in 4% formaldehyde, paraffin sections were then prepared and stained with H&E. **A** Sham control; **B** Vehicle control; **C** gp120/NRG-1 (10 mg/kg); **D** JK07 (1 mg/kg); **E** JK07 (3 mg/kg); **F** JK07 (10 mg/kg).

Table 4 | Effect of JK07 on myocardial collagen type I/III expression (Mean ± SD)

Group	Collagen I (%)	Collagen III (%)	Collagen I/III Ratio
Sham Control	0.9 ± 0.29	1.18 ± 0.24	0.78 ± 0.28
Vehicle Control	10.09 ± 2.18$^{\triangle\triangle\triangle}$	5.44 ± 1.1$^{\triangle\triangle\triangle}$	1.91 ± 0.52$^{\triangle\triangle\triangle}$
JK07 (1 mg/kg)	9.42 ± 0.81	5.5 ± 1.56	1.82 ± 0.48
JK07 (3 mg/kg)	6.35 ± 3.25*	5.15 ± 2.39	1.13 ± 0.29*
JK07 (10 mg/kg)	6.00 ± 1.22**	5.13 ± 1.95	1.21 ± 0.23*
gp120-NRG1 Fusion	6.41 ± 0.14**	5.43 ± 1.19	1.22 ± 0.29*

Note: 1. $^{\triangle\triangle\triangle}p < 0.01$ denotes statistical significance in comparison to the sham control.
2. $^{*}p < 0.05$, $^{**}p < 0.01$ denotes statistical significance in comparison to the vehicle control

dysfunction classification system (Fig. 6A). Similar to the HFrEF study, no changes were observed during the course of the study in animals treated with vehicle control (Fig. 6B). Unlike with HFrEF, treatment with JK07 and sacubitril/valsartan showed profoundly different responses. Treatment with JK07 resulted in improvement by at least one class of diastolic dysfunction in six out of ten animals treated (Supplementary Tables 1 and 2). In contrast, only one of ten animals treated with sacubitril/valsartan showed at least one class of diastolic dysfunction. No significant changes in NTproBNP were observed across treatment groups.

Discussion

This research characterizes JK07, an NRG1-based molecule biased to induce HER4 signaling preferentially over HER3 signaling. The preferential activation of HER4 is achieved through molecular fusion of the EGF-binding domain of NRG-1 to the C-terminus of an antagonistic antibody specific for HER3. Preferential HER4 activation by JK07 is validated in vitro and in vivo. JK07 is subsequently shown to induce potent improvement in myocardial function as well as anti-cancer activity in vivo. Included in this work is a direct comparison demonstrating that a control molecule (gp120 mAb/NRG1 fusion) able to activate HER3 and HER4 equally well, shows no therapeutic benefit beyond JK07. Biased HER4 activation by JK07 is shown to be sufficient for potent improvement in myocardial function in a rhesus macaque model of heart failure, in the setting of both reduced and preserved ejection fraction. Taken together, this research, for the first time, demonstrates that activation of HER4 preferentially can catalyze the potent positive cardiac remodeling and antifibrotic effects of rNRG-1 and portends a potentially more favorable approach to the use of rNRG as a therapeutic in the treatment of heart failure, In addition to the demonstration that JK07 can induce meaningful improvements in myocardial function, this work also demonstrated JK07-mediated tumor growth inhibition in a relevant xenograft model of cancer sensitive to HER3 signaling. This juxtaposition could profoundly change the potential risk profile for the use of NRG-1 as a therapeutic.

Prior to this work, the role of HER3 stimulation in the neuregulin-mediated improvement in myocardial function was not clear. The demonstration that JK07 improves ejection fraction in a rodent LAD ligation model to the same degree as a control molecule (gp120 mAb/NRG1 fusion) with an antibody unable to block HER3 signaling supports that HER4 is the major, if not exclusive, pathway responsible for the myocardial effects. Conversely, in the FaDu xenograft model, HER3 appears to be exclusively responsible for the tumor growth, as evidenced by the high degree of efficacy demonstrated with the anti-HER3 antibody. Although the tumor growth inhibition was dose-dependent for JK07 across all three dose levels evaluated, the high dose of JK07 did not demonstrate as much tumor burden reduction as the HER3 antibody. Further, in contrast to the above findings, in vitro evaluation of JK07 in cancer cell proliferation assays showed attenuated but not abrogated HER3 activity. Further studies will be necessary to fully elucidate the individual roles of HER3 and HER4 in treating myocardial dysfunction.

Recently, a large-scale multi-omics approach to evaluate key drivers of heart failure with reduced ejection fraction revealed four major pathways contributing to pathogenesis, all of which fall under the HER2 signaling pathway and are potentially able to be modulated through neuregulin activation. This interrogation of clinical data reinforces the results of studies with JK07 and its potential as a therapeutic intervention for heart failure. In this work, we demonstrate activation of the PI3K-AKT pathway both

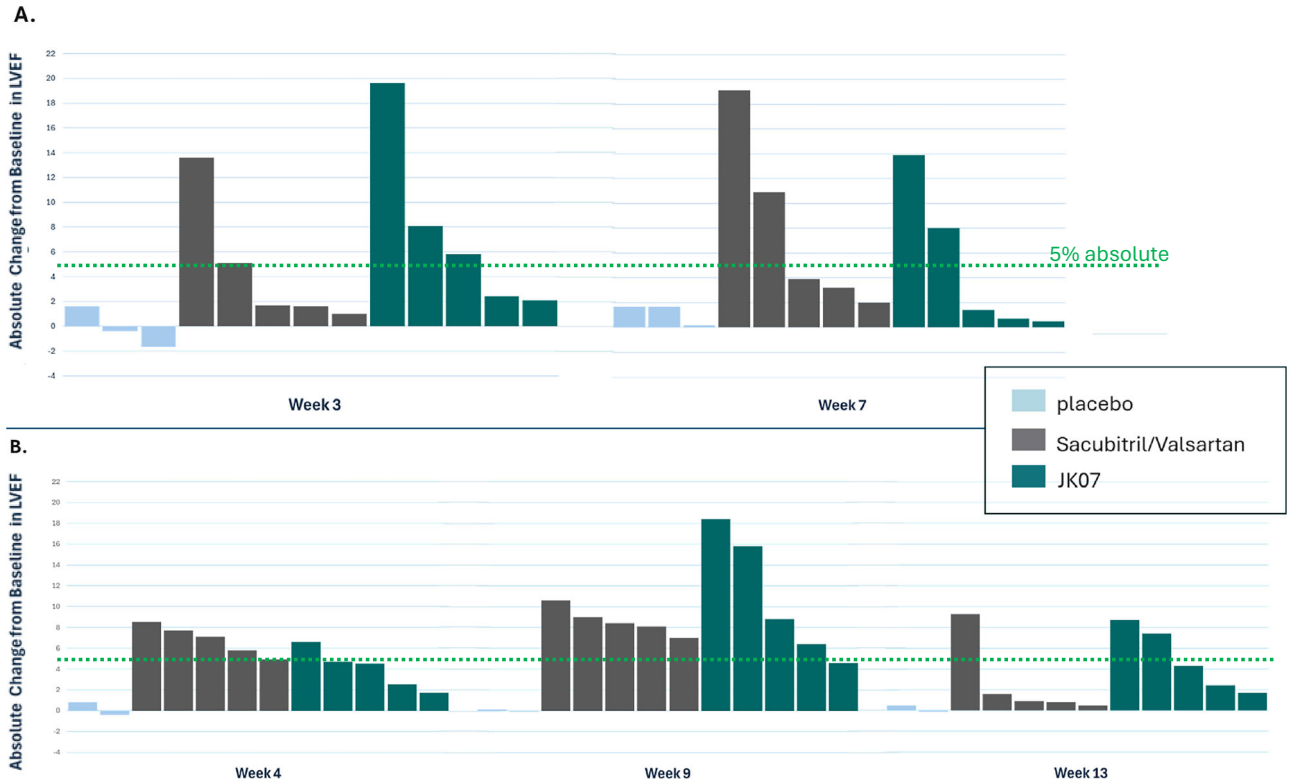

Fig. 5 | Evaluation of JK07 in a Rhesus Macaque Model of Heart Failure with Reduced Ejection Fraction. *Denotes statistically significant difference as compared to baseline by paired t-test ($p < 0.05$). Effects of treatments on left ventricular ejection fraction in rhesus macaques with HFrEF (spontaneous HF model). **A** Study 1: Animals received two, QW doses of JK07 or daily doses of Sacubitril/Valsartan for 7 weeks. Meaningful increase (defined as >5% absolute change from baseline, CFB, dashed green line) in LVEF observed in 3/5 JK07-treated animals at week 3 and 2/5 JK07-treated animals at week 7 (week 7 is 6 weeks after last dose of JK07). **B** Study 2: Rhesus Macaques (spontaneous HF model) received nine, QW doses of JK07 or daily doses of Sacubitril/Valsartan for 9 weeks. Meaningful increase in LVEF observed in 3/5 JK07-treated animals at week 4 and 4/5 JK07-treated animals at week 9. At week 13, 4 weeks following the last dose of JK07, 3/5 animals continued to demonstrate LVEF > 5% absolute increase from baseline.

in vitro and ex vivo, which was one of the pathways identified by Ouwerkerk et al.

The rodent LAD ligation model presented here demonstrates that JK07 can improve exercise capacity in addition to the improvement in echocardiographic parameters. This study showed significant toxicity in rodents receiving repeated administrations of JK07, which was not observed in monkeys receiving repeated administrations. Previous research has shown that NRG-1 can induce species-specific hypoglycemic effects[26], and separate studies with JK07 have shown that these hypoglycemic effects can be profound and lethal at higher doses with shorter dose intervals in rodents (data not shown), but no hypoglycemia has been observed in non-human primates or in clinical studies with JK07 to date. The observation that the improvement in exercise endurance was not dose-dependent may relate to the more potent induction of hypoglycemia at the higher dose levels, as hypoglycemia could have impacted animal performance in the exercise capacity assessments.

Results presented here extend recent findings of a small molecule activator or HER4[27]. In that work, a small molecule activator selective for HER4 dimerization named EF-1 was identified and evaluated for its ability to induce effects similar to NRG-1 in vitro and in vivo. Like NRG-1, and as presented here for JK07, EF-1 was able to elicit protection against heart failure and fibrosis. As with JK07, the selectivity for HER4 demonstrated for EF-1 was relative rather than absolute. As such, both JK07 and EF-1 independently demonstrate that HER4 selective agonism can yield meaningful improvements in heart structure and function, despite differing ways of achieving selectivity and differing selectivity profiles.

Published clinical studies employing neuregulin as a potential treatment for heart failure have exclusively focused on heart failure with reduced ejection fraction, despite evidence of neuregulins possessing anti-fibrotic effects and a purported role for fibrosis in heart failure with preserved ejection fraction. In this work, we not only show improvement in fibrosis in a rodent model of heart failure but also demonstrate clear improvement in diastolic dysfunction in a spontaneous model of heart failure in rhesus macaques. In this model, sacubitril/valsartan treatment exhibited a substantially greater benefit in HFrEF animals than in HFpEF animals, the latter in which only one animal demonstrated response, consistent with the relative benefit observed in clinical trials.

Taken together, JK07 represents a promising new treatment for HFrEF and HFpEF and is currently being evaluated in a Phase 2 study recruiting both HFrEF and HFpEF subjects (RENEU-HF; NCT06369298.). One limitation of these studies is that they did not assess how JK07 may work incrementally to the number of available treatment options used for heart failure currently. Another limitation of these studies is that JK07 has a lower affinity for rodent HER3 than for primate and human HER3 (approximately 10-fold lower, data not shown), which may have affected the results of the LAD ligation model. Finally, the non-human primate model of spontaneous heart failure reflects a heterogeneous group of animals due to the spontaneous nature of the disease, and therefore results of future studies could differ more so than with an artificially-induced model system. In the in vivo studies presented here, only male animals were used, so the potential impact of hormonal differences on the outcomes of these studies will need to be evaluated in the future.

Methods

Experimental Animals

All animal experimentation was conducted in accordance with the standards of the Association for Assessment and Accreditation of Laboratory Animal Care International (AAALAC).

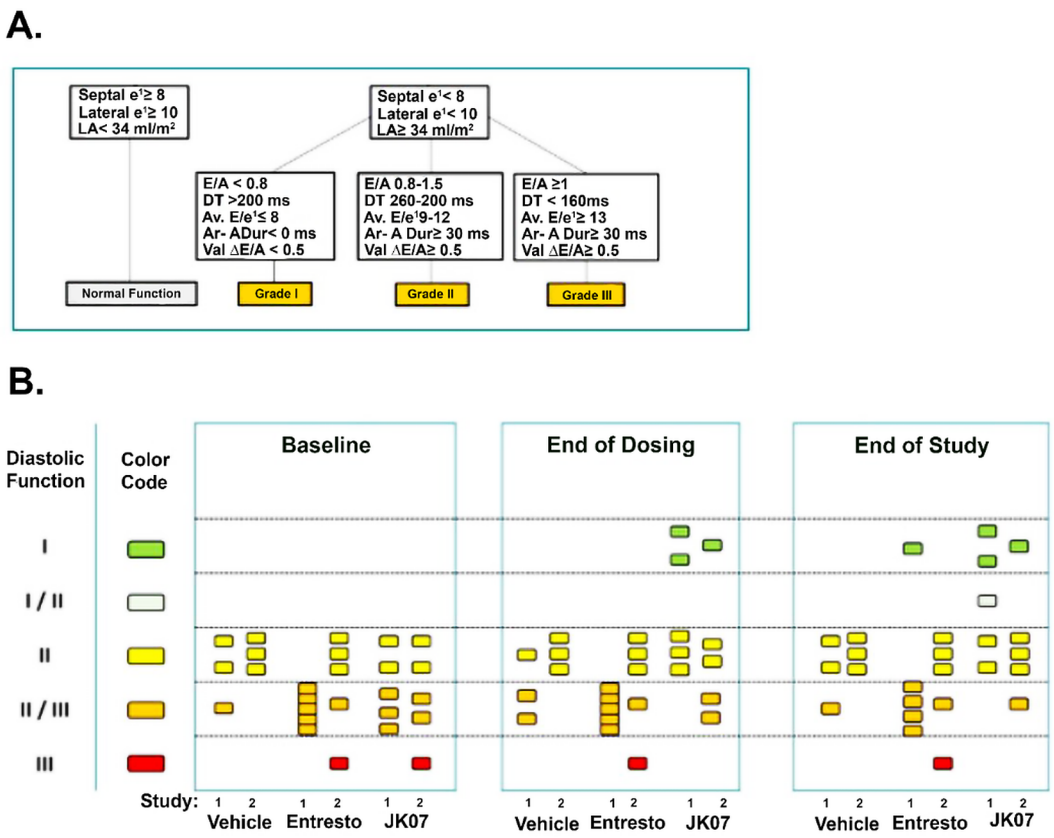

Fig. 6 | Evaluation of JK07 in a Rhesus Macaque Model of Heart Failure with Preserved Ejection Fraction. Effects of treatments on diastolic function in rhesus monkeys with HFpEF (Supplementary tables 1 and 2).

Mice. NOD/SCID mice (17.5–21.5 g) from Beijing AK Bio-Technology Co. Ltd. (Beijing, China) were used (animal certificate number: 1140240001273). The experimental protocol was conducted by Crown-Bio International R&D Center (Beijing, China), an AAALAC accredited Contract Research Organization. The final study protocol and report was audited and approved by the CrownBio IACUC Committee. The experiment was performed according to the requirements of AAALAC.

Rats. The experimental protocol was conducted by Tianjin Pharmaceutical Research Institute of New Drug Evaluation Co., Ltd. (Tianjin, China), an AAALAC accredited Contract Research Organization. Male Sprague Dawley rats (273–315 g) from Beijing Vital River Laboratory Animal Technology Co., Ltd., Bejing, China) were used (supplier license number: SCXK (Beijing) 2016-0006).

Monkeys. *Macaca mulatta* male monkeys ($n = 26$; age 12–23 years) (Ya'an Primed Biological Technology Co., Ltd., Sichuan, China) were maintained on a 12-hour light/dark cycle and were fed four times a day at the testing facility, Sichuan Primed Shines Bio-tech Co., Ltd. (Chengdu, China), AAALAC accredited Contract Research Organization. Monkeys were divided into three JK07 treatment groups: two weekly IV injections of 1 mg/kg JK07 ($n = 10$ total), daily oral administration of 6.6 mg/kg/day sacubitril/valsartan for 49 days ($n = 10$ total), or two weekly IV injections of PBS ($n = 6$). Groups were equally divided between monkeys with HFrEF and HFpEF. All monkeys had abnormal glucose and lipid metabolism for at least 3 years, normal blood pressure or grade 1 hypertension, had HFpEF, including diastolic dysfunctional characteristics of e'<8, E/e'>8, and grade II diastolic dysfunction ($n = 13$) or HFrEF, including systolic dysfunctional characteristics of LVEF at 30–51% and cardiac remodeling. Animals were anesthetized by intramuscular injection of 15 mg/kg ketamine hydrochloride prior to undergoing echo. No animals were euthanized at any point during or after completion of this study.

The treatment duration and evaluation intervals differed between the two studies. In the first study, treatment consisted of JK07 or vehicle administered intravenously once weekly for two consecutive weeks, with JK07 administered at a dose level of 1.0 mg/kg, and sacubitril/valsartan at the human equivalent dose of 3.3 mg/kg/day for Days 0-6 and 6.6 mg/kg/day thereafter until the final evaluation at 7 weeks. Echocardiographic evaluations were performed at week 3 (the week of the final administration of JK07) and at week 7 (five weeks after the final administration of JK07). In the second study, treatment consisted of JK07 or vehicle administered intravenously once weekly for nine consecutive weeks, with JK07 administered at a dose level of 0.1 mg/kg for the first five weeks and 0.3 mg/kg for the last four weeks. In the second study, sacubitril/valsartan was given at the human equivalent dose of 3.3 mg/kg/day for Days 0–6 and 6.6 mg/kg/day thereafter through week 9 of the study.

Cell Culture

Cancer Cell Lines. All cancer cell lines were obtained from ATCC, except the human bladder tumor cell line RT-112 which was provided by DSMZ. Human NCI-N87 gastric carcinoma (CRL-5822, ATCC, Manassas, VA), T-47D breast carcinoma (HTB-133, ATCC), and RT-112 urinary bladder transitional cell carcinoma (ACC 418, Leibniz Institute DSMZ, Braunschweig, DE) were cultured under standard culture conditions. Human breast cancer cell line MCF-7 and rat bladder tumor cell line NBT-II were maintained in EMEM medium supplemented with 10% heat-inactivated fetal bovine serum (FBS). Monkey lung/bronchus epithelial cell line 4MBr-5 was maintained in Ham's F-12K Medium supplemented with 30 ng/ml murine EGF (BD Bioscience) and 10% heat-inactivated FBS. All cancer cell lines were cultured in the presence of 1%

antibiotics penicillin-streptomycin and in a humidified atmosphere of 5% CO_2 at 37 °C.

Human Cardiomyocytes. Induced human pluripotent stem cell-derived cardiomyocytes were prepared according to the manufacturer's protocol (iCell®, FUJIFILM Cellular Dynamics, Madison, WI). Briefly, cells were suspended at 5×10^5 cells/ml and seeded at 1 mL/well in a 0.1% gelatin-coated culture plate. The cells were incubated at 37 °C/5% CO_2 for 4 h to allow adhesion to the plate, and unattached cells and debris were removed by replacing the medium. Cells were cultured for approximately one week at 37 °C/5% CO_2, with medium refreshed every other day to allow differentiation into functional cardiomyocytes.

Neonatal Rat Ventricular Myocytes. Neonatal rat ventricular myocytes were maintained in culture according to manufacturer's recommendations (Clonetics™, Lonza, Basel, CH). Cells were suspended at 4×107 cells/mL and seeded at 1 mL per well in a nitrocellulose-coated culture plate. The resulting cell density was about 4×10^5 cells/well. After 4 h of incubation at 37 °C/5% CO_2, approximately 80% of the medium was replaced with fresh pre-warmed medium containing 200 μM BrdU (Lonza). Medium was refreshed every other day to allow differentiation.

U2OS Dimerization Cell Lines. Both PathHunter® U2OS HER2/HER4 and U2OS HER2/HER3 dimerization cell lines were obtained from Eurofins DiscoverX under a material transfer agreement. Cells were cultured at 37 °C/5% CO_2 using the AssayComplete cell culture kit 103 (Eurofins DiscoverX, Fremont, CA) supplemented with 250 μg/mL Hygromycin B and 500 μg/mL G418. Cells were maintained at 30–90% confluence by passaging every 2-3 days at no more than 1:3 split ratio using AssayComplete cell detachment reagent (Eurofins DiscoverX).

FaDu Cell Line. FaDu cells were cultured in MEM plus 0.01 mM NEAA medium supplemented with 10% fetal bovine serum at 37 °C in an atmosphere of 5% CO_2 in air. Cells growing in the exponential growth phase were harvested and used for tumor inoculation.

In Vitro Binding Activity and Specificity

Structural Integrity. To examine the structural integrity of JK07 molecule, surface plasmon resonance (SPR) binding experiments were performed using Biacore 8 K systems (GE HealthCare, Chicago, IL). HBS-EP+ buffer (10 mM HEPES, 150 mM NaCl, 3 mM EDTA, and 0.05% v/v Surfactant P20) was used as the running buffer. Anti-His antibody was coupled in active flow cells on a CM5 sensor chip using amine coupling kit (GE Healthcare), whereas the reference cell was left blank. As the first step, His-tagged HER3 (Sino Biological, Wayne, PA) was injected over both cells on all experimental channels. Secondly, test articles JK07, HER3 antagonist antibody, or buffer were injected over both cells on the corresponding channel. Third, anti-NRG1 antibody (R&D Systems, Minneapolis, MN) was injected over both cells on all experimental channels. After each binding cycle, the sensor chip was regenerated with 50 mM NaOH plus 1 M NaCl. SPR signals (RU) were recorded in real time and plotted against time to generate binding sensorgrams. Sensorgrams from multiple channels were overlaid using Biacore™ 8 K Control Software (Biacore International AB, Upsala, SE).

Target Binding Affinity. The binding affinity of JK07 to HER3 across species was measured by Biacore kinetic experiments using a Protein A sensor chip on Biacore 8 K (GE HealthCare) with HBS-EP+ as running buffer. JK07 was captured to a target level of around 100RU on the active cell of a protein A sensor chip. HER3 proteins from different species were serially diluted to 14, 7, 3.5, 1.75, and 0.875 nM with HBS-EP+ buffer and injected over surfaces of both active and reference cells at a flow rate of 40 μL/min. HER3 from human, monkey, rat, and mouse were tested simultaneously over individual channels on the same sensor chip. After each binding cycle, the sensor chip was regenerated with 50 mM NaOH plus 1 M NaCl. Signals from reference surface and an ensemble of buffer blank injections were subtracted from binding signals to correct for nonspecific binding and injection artifacts. The corrected experimental signals were globally fitted to a 1:1 binding model to extract kinetic constants, including association rate constant (ka), dissociation rate constant (kd), and equilibrium dissociation constant rate constant (KD), using the Biacore 8 K Evaluation Software.

In Vitro Assays

ELISA. To detect AKT phosphorylation following receptor activation, cells cultured in 96-well plates were starved for 4 hours in serum-free medium containing 0.1% BSA and then stimulated with JK07 or control articles at 37 °C/5% CO_2 for 15 minutes. Cells were washed twice with ice-cold PBS and then lysed in the cell lysis buffer containing a protease/phosphatase inhibitor cocktail (Cell Signaling Technology, Danvers, MA). Phospho-AKT and total AKT in the cell lysates were measured by ELISA using the RayBio® Phospho-AKT (Ser473) and Total AKT ELISA kits according to the manufacturer's protocols. Data were analyzed using the GraphPad Prism software and presented as the relative ratio of phospho-AKT to total-AKT which is normalized by the medium control.

Proliferation Assay. Human cancer cell lines NCI-N87, RT-112, T-47D, and MCF-7 were plated in serum-free media containing 0.1% BSA at a density of 5000 to 10,000 cells per 100 μL per well, depending on the growth kinetics of each cell line, in 96-well flat bottom plates. JK07 or control articles were prepared at 2x working concentration in a stepwise 1:4 serial dilution series using the culture medium, then added to the cells at 100 μL/well in triplicates. Cells were incubated at 37 °C/5% CO2 for 5 days. Cell viability was determined using CCK-8 (Dojindo Molecular Technologies) in accordance with the manufacturer's instructions. Data were analyzed using the GraphPad Prism software and presented as the relative rate of growth normalized by the medium control.

Western Blots. To examine AKT phosphorylation upon JK07 stimulation in iCell® human cardiomyocytes and rat primary cardiomyocytes, cells were cultured at 37 °C/5% CO_2 for approximately one week per the manufacturer's instructions to allow full differentiation and then stimulated with JK07 or control articles at a concentration of 16 nM at 37 °C for 15 min. At the end of treatment, cells were washed twice with ice-cold PBS and then lysed in RIPA lysis buffer (Thermo Fisher Scientific, Waltham, MA) containing protease and phosphatase inhibitors (Cell Signaling Technology). Protein concentrations in the cell lysates were determined by Thermo Fisher Scientific's BCA assay according to manufacturer's protocol. SDS-PAGE was carried out using the Invitrogen NuPAGE® system. Briefly, cell lysates were mixed with 4x NuPAGE® LDS Sample Buffer and NuPAGE® Sample Reducing Agent and heated at 95 °C for 5 min. Treated cell lysates normalized for protein content were loaded onto a NuPAGE™ 4–12% Bis-Tris gel and run at 100 V constant voltage. At the end of electrophoresis, proteins were transferred onto the iBlot gel nitrocellulose membrane. The membrane was blocked for 1 h with 5% nonfat dry milk and then immunoblotted using the iBind Flex Western Device™ (Invitrogen, Waltham, MA) with rabbit anti-HER4/HER4 antibody (111B2), or rabbit anti-phospho-HER4/HER4 (Tyr1284) antibody (21A9), or rabbit anti-AKT antibody, or rabbit anti-phospho-AKT (Ser473) antibody, followed by the HRP-labeled goat anti-rabbit antibody (Cell Signaling Technology). The membrane was washed and incubated with SuperSignal™ West Pico PLUS (Thermo Fisher Scientific) or Femto Chemiluminescent Substrate, and then detected by iBright CL1000 Imaging System (Thermo Fisher Scientific).

Animal Models

FaDu Mouse Model. Mice were injected subcutaneously in the right flank with FaDu hypopharyngeal squamous cell carcinoma cells (3×10^6)

suspended in 0.1 mL of PBS to establish the tumor xenografts. Mice were staged and randomized to treatment or vehicle when the mean tumor volume reached approximately 150 mm3. Randomization was performed using a deterministic distribution based on tumor volume. The animals were sorted to normalize tumor volume and assigned to the corresponding experimental groups. At the initiation of treatment, treatment or control was administered to the tumor-bearing mice via tail vein injection. After the tumor inoculation, animals were monitored daily for general health/morbidity and mortality. At the time of daily routine check, animals were examined for behaviors including mobility, food and water consumption (by visual estimation), body weight gain/loss (body weights were measured twice a week), eye health, hair matting, and any other visible abnormalities. Animal death and the frequency of observation of clinical signs, if any, were recorded for each experimental group.

Tumor volumes were measured twice a week in two dimensions using a caliper. The tumor volume was calculated in mm3 using the following formula: V = 0.5a x b2, where a and b were the length and width of the tumor, respectively. Tumor weight was measured at the end of the study after the mice were euthanized via CO2 inhalation followed by cervical dislocation. Tumor growth inhibition was calculated as follows: TGI (%) = 1 - T/C, where T and C are the mean relative tumor volume (RTV) or mean tumor weight in the treatment group and the control group, respectively. RTV = Vt/V0, V0 is the tumor volume on the day of the first dose administration, Vt is the tumor volume after the subsequent dose administration.

Rodent Heart Failure Model. Sprague-Dawley rats were anesthetized with an intraperitoneal injection of 60 mg/kg of 3% pentobarbital sodium. The anesthetized animals were placed in a supine position on the operating desk, and the chest hair was shaved from the surgical area. Following the standard disinfection procedures, the rats were sequentially subjected to skin and muscle incision and muscle external purse-string suture. Left-sided thoracotomy was performed between the third and fourth intercostal spaces. The heart was gently pulled out using a ring hook. A 6-0 silk suture thread was placed underneath the left anterior descending (LAD) coronary artery and tied at a position of 3–4 mm below the left atrial appendage. The heart was placed back into the thoracic cavity, and the wound was closed. The air left in the thoracic cavity was evacuated to allow re-inflation of the lungs. The muscle and skin were sutured. In the sham control group, animals underwent the same surgical procedures with the exception that the LAD coronary artery was not ligated by the silk suture thread. Transthoracic echocardiographic images of hearts from all rats were obtained before the surgery and 4 weeks after the LAD ligation, respectively, using a Doppler high-resolution ultrasound scanner (Vevo 770-120, Visual Sonics, Toronto, CA) to evaluate the cardiac function. Ejection fraction was determined with the M-mode echocardiography. LAD-ligated animals with a more than 30% decrease in EF were selected and used in this study.

Four weeks after the LAD ligation, animals with heart failure and reduced EF (> 30% decrease) were randomized and assigned into five groups with 11 animals per group as follows: vehicle control group, JK07 groups at 1, 3 and 10 mg/kg, and positive control group. Ten animals undergoing sham surgery were included in the sham control group. Animals in the vehicle control group and the sham control group were administered PBS (vehicle); animals in the JK07 groups were administered 1, 3, or 10 mg/kg of JK07; animals in the positive control group were administered 10 mg/kg gp120 mAb/NRG-1 fusion protein. All experimental articles were administrated via tail vein injection with a volume of 2 mL/kg. All animals received administrations twice per week for up to four weeks. Animals were euthanized by CO2 inhalation followed by cervical dislocation.

Echocardiography in Rodents. Animals were anesthetized with 15 mg/kg ketamine hydrochloride. Doppler echocardiography was recorded from each animal at 17.5 MHz using Vevo 770TM-120 Imaging System at the following time points: before the LAD ligation surgery, before the treatment, 2-week and 4-week post-treatment. Images from a short axis view of the left ventricle at the M-mode were collected and analyzed by software to determine the following parameters: interventricular septum thickness at end-diastole (IVSd), interventricular septum thickness at end-systole (IVSs), left ventricular posterior wall thickness at end-diastole (LVPWd), left ventricular posterior wall thickness at end-systole (LVPWs), LVIDd, and LVIDs.

Endurance test in Rodents. Four weeks after the first administration, the exercise endurance of each animal was examined in a running wheel, and the running distance in 10 minutes was recorded. Lead II electrocardiogram (ECG-II) was recorded from each animal before the treatment (pre-treatment) and at 4 weeks post-treatment (W4), respectively. Heart rate (bpm), the depth of Q wave (mv), the width of Q wave (s), the height of ST interval (mv) and QT duration (s) were monitored. Four weeks after the first administration, the parameters of systolic arterial pressure, diastolic arterial pressure, mean arterial pressure, and heart rate (HR) were measured following the insertion of SPR-320NR(2 F) Millar pressure catheters into the right carotid artery. The maximum rate of increase of left ventricular pressure ($+LVdP/dt_{max}$), maximum rate of decrease of left ventricular pressure ($-LVdP/dt_{max}$), left ventricular systolic pressure (LVSP), and left ventricular end-diastolic pressure (LVEDP) were measured by inserting the pressure catheters into the left ventricle. These parameters were collected by MP150 multi-channel physiological signal acquisition system and analyzed by AcqKnowledge v.3.9.1 software (BIOPAC Sytems, Inc., Goleta, CA). Four weeks after the first administration, the rat hearts were dissected and frozen at -20 °C following a wash in saline. Five hearts in each experimental group were evaluated for infarct size measurements. The heart tissues under the ligation site were sectioned in 1-mm thickness, and then stained with 2% triphenyltetrazolium chloride solution at 37 °C for 1 min. The infarct size, determined as a percentage of left ventricular surface area, was analyzed using a pathological image analysis system. Four weeks after the first administration, the heart tissues from each group were collected, washed with saline, and then fixed in 4% formaldehyde. The tissues surrounding the coronary artery under the ligation site were embedded in paraffin. Five-μm thick paraffin sections were prepared and stained with hematoxylin and eosin. Histopathological changes were assessed by light microscopy. Four weeks after the first administration, the heart tissues from each group were collected, washed with saline, and then fixed in 4% formaldehyde. The tissues surrounding the coronary artery under the ligation site were embedded in paraffin. Five-μm thick paraffin sections were prepared and stained with a biotinylated antibody specific for Collagens I or III, followed by horseradish peroxidase-labeled streptavidin, to detect the type I/III collagen deposition in the heart tissue. Two fields of view from each slide were randomly selected to estimate the positively-stained areas under a light microscope (10×40). Data are presented as the mean percentage of collagen-positive area in the total area.

Monkey Heart Failure Model. The Primed Primate Research Center (Chengdu, China) has built up a clinical dynamic database on a 7-year history of disease progression of more than 800 rhesus monkeys with primary metabolic disorders. This database maintains records from a comprehensive list of metabolic indicators, such as fasting plasma glucose, blood pressure, triglyceride, total cholesterol, low-density lipoprotein cholesterol, and high-density lipoprotein cholesterol. In addition, the records of cardiac diastolic and systolic functions of more than 300 monkeys have been obtained by echocardiography (2D ultrasound, M model, Simpson's method, color M model, tissue Doppler, mitral blood flow, pulmonary venous blood flow, etc.).

Twenty-six middle-aged or old-aged male *Macaca mulatta* monkeys with spontaneous chronic heart failure were included according to the following inclusion criteria: (1) aged 12–24 years (equivalent to humans aged 40-70 years), with abnormal glucose and lipid metabolism for at least 3

years; (2) normal blood pressure or Grade 1/2 hypertension; (3) either HFpEF, including diastolic dysfunctional characteristics of e'<8, E/e'>8 and grade II-III diastolic dysfunction (DD2-DD3) (13 monkeys), or HFrEF, including systolic dysfunctional characteristics of LVEF at 30-51% and cardiac remodeling (13 monkeys). Enrolled animals were assigned into three groups: (1) 10 animals (5 for each of HFrEF and HFpEF) in the JK07 group, receiving weekly intravenous injection of JK07 at 1 mg/kg for a total of two injections; (2) 10 animals (5 for each of HFrEF and HFpEF) in the sacubitril/valsartan group, receiving daily oral administration of sacubitril/valsartan at the clinical-equivalent dose (6.6 mg/kg/day) for a total of 49 days (7 weeks); and (3) six animals (3 for each of HFrEF and HFpEF) in the placebo group, receiving weekly intravenous injection of PBS for a total of two injections. The primary endpoint was systolic function and diastolic function evaluated by echocardiography. The secondary endpoints included blood pressure, blood chemistry panel containing glucose and lipid metabolism, safety index, hematology, body weight, food consumption, and clinical observations. Echocardiography, blood pressure, NT-proBNP, and blood chemistry panels were performed once before and twice after treatment. Hematology tests were carried out once before and once after treatment. Body weight was measured once a week. Food consumption and clinical observations were recorded daily throughout the study. Data from the individual animal's cardiac function tests were compared to the corresponding baseline by paired t-test. Difference is considered statistically significant if $p < 0.05$.

Data Availability

All source data are stored centrally on an access-restricted cloud platform managed by Salubris Biotherapeutics, Inc. Data requests should be directed to Salubris Biotherapeutics, Inc.

Received: 12 December 2024; Accepted: 15 January 2026;
Published online: 02 March 2026

References

1. Heidenreich, P. A. et al. 2022 AHA/ACC/HFSA Guideline for the Management of Heart Failure: a report of the American College of Cardiology/American Heart Association Joint Committee on Clinical Practice Guidelines. *Circulation* **145**, e895–e1032 (2022).
2. Roger, V. L. Epidemiology of heart failure: a contemporary perspective. *Circ. Res.* **128**, 1421–1434 (2021).
3. Savarese, G. et al. Global burden of heart failure: a comprehensive and updated review of epidemiology. *Cardiovasc. Res.* **118**, 3272–3287 (2023).
4. Rupert, C. E. & Coulombe, K. L. The roles of neuregulin-1 in cardiac development, homeostasis, and disease. *Biomark. Insights* **10**, 1–9 (2015).
5. Parodi, E. M. & Kuhn, B. Signalling between microvascular endothelium and cardiomyocytes through neuregulin. *Cardiovasc. Res.* **102**, 194–204 (2014).
6. Tzahar, E. et al. ErbB-3 and ErbB-4 function as the respective low and high affinity receptors of all Neu differentiation factor/heregulin isoforms. *J. Biol. Chem.* **269**, 25226–25233 (1994).
7. Bouyain, S., Longo, P. A., Li, S., Ferguson, K. M. & Leahy, D. J. The extracellular region of ErbB4 adopts a tethered conformation in the absence of ligand. *Proc. Natl. Acad. Sci. USA* **102**, 15024–15029 (2005).
8. Chen, X. et al. An immunological approach reveals biological differences between the two NDF/heregulin receptors, ErbB-3 and ErbB-4. *J. Biol. Chem.* **271**, 7620–7629 (1996).
9. Pentassuglia, L. & Sawyer, D. B. The role of Neuregulin-1beta/ErbB signaling in the heart. *Exp. Cell Res.* **315**, 627–637 (2009).
10. Bouwer, N. I. et al. Cardiac monitoring in HER2-positive patients on trastuzumab treatment: a review and implications for clinical practice. *Breast* **52**, 33–44 (2020).
11. Kimball, A. et al. Late characterisation of cardiac effects following anthracycline and trastuzumab treatment in breast cancer patients. *Int J. Cardiol.* **261**, 159–161 (2018).
12. Smith, I. et al. 2-year follow-up of trastuzumab after adjuvant chemotherapy in HER2-positive breast cancer: a randomised controlled trial. *Lancet* **369**, 29–36 (2007).
13. Zurek, M. et al. Neuregulin-1 induces cardiac hypertrophy and impairs cardiac performance in post-myocardial infarction rats. *Circulation* **142**, 1308–1311 (2020).
14. Liu, X. et al. Neuregulin-1/erbB-activation improves cardiac function and survival in models of ischemic, dilated, and viral cardiomyopathy. *J. Am. Coll. Cardiol.* **48**, 1438–1447 (2006).
15. Doggen, K. et al. Ventricular ErbB2/ErbB4 activation and downstream signaling in pacing-induced heart failure. *J. Mol. Cell Cardiol.* **46**, 33–38 (2009).
16. Galindo, C. L. et al. Neuregulin (NRG-1beta) is pro-myogenic and anti-cachectic in respiratory muscles of post-myocardial infarcted swine. *Biology* **11**, https://doi.org/10.3390/biology11050682 (2022).
17. Lenihan, D. J. et al. A Phase I, single ascending dose study of cimaglermin Alfa (Neuregulin 1beta3) in patients with systolic dysfunction and heart failure. *JACC Basic Transl. Sci.* **1**, 576–586 (2016).
18. Jabbour, A. et al. Parenteral administration of recombinant human neuregulin-1 to patients with stable chronic heart failure produces favourable acute and chronic haemodynamic responses. *Eur. J. Heart Fail* **13**, 83–92 (2011).
19. Majumder, A. HER3: toward the prognostic significance, therapeutic potential, current challenges, and future therapeutics in different types of cancer. *Cells* **12**, https://doi.org/10.3390/cells12212517(2023).
20. Segers, V. F. M., Dugaucquier, L., Feyen, E., Shakeri, H. & De Keulenaer, G. W. The role of ErbB4 in cancer. *Cell Oncol. (Dordr.)* **43**, 335–352 (2020).
21. Laskin, J. et al. NRG1 fusion-driven tumors: biology, detection, and the therapeutic role of afatinib and other ErbB-targeting agents. *Ann. Oncol.* **31**, 1693–1703 (2020).
22. Shin, D. H., Jo, J. Y. & Han, J. Y. Dual targeting of ERBB2/ERBB3 for the treatment of SLC3A2-NRG1-mediated lung cancer. *Mol. Cancer Ther.* **17**, 2024–2033 (2018).
23. Gan, H. K. et al. A Phase I, first-in-human study of GSK2849330, an anti-HER3 monoclonal antibody, in HER3-expressing solid tumors. *Oncologist* **26**, e1844–e1853 (2021).
24. Vermeulen, Z., Segers, V. F. & De Keulenaer, G. W. ErbB2 signaling at the crossing between heart failure and cancer. *Basic Res Cardiol.* **111**, 60 (2016).
25. Alvarado, D. et al. ErbB activation signatures as potential biomarkers for anti-ErbB3 treatment in HNSCC. *PLoS One* **12**, e0181356 (2017).
26. Huang, Z. et al. Species-specific effects of neuregulin-1beta (cimaglermin alfa) on glucose handling in animal models and humans with heart failure. *Toxicol. Appl. Pharm.* **332**, 92–99 (2017).
27. Cools, J. et al. Small-molecule-induced ERBB4 activation to treat heart failure. *Nat. Commun.* **16**, 576 (2025).

Acknowledgements

The authors thank Shenzhen Salubris Pharmaceuticals, Co. Ltd. For funding of the work.

Author contributions

S.L.M. contributed to analysis of data and authorship of the manuscript. W.H.W.T. contributed to analysis of data and authorship of the manuscript. X.Z. performed the experiments and analyzed the data. J.L. conceived and designed the experiments and contributed to analysis of data.

Competing interests

The Authors declare no Competing Non-Financial Interests but the following Competing Financial Interests: Samuel L. Murphy, Xiaolei Zhuang, and John Li were employees of Salubris Biotherapeutics, Inc. at the time the studies described in this paper were conducted.

Additional information

Supplementary information The online version contains supplementary material available at https://doi.org/10.1038/s44386-026-00038-5.

Correspondence and requests for materials should be addressed to Samuel L. Murphy.